Journal of Physics:
Condensed Matter



**PAPER** • **OPEN ACCESS**

# Structure and motion of tritium and helium in the breeding-blanket-relevant liquid lithium–lead eutectic alloy: *ab-initio* molecular dynamics simulations

To cite this article: Beatriz G del Rio *et al* 2026 *J. Phys.: Condens. Matter* **38** 135401

Journal of Physics: Condensed Matter



OPEN ACCESS

RECEIVED
30 December 2025

REVISED
2 March 2026

ACCEPTED FOR PUBLICATION
25 March 2026

PUBLISHED
2 April 2026



PAPER

# Structure and motion of tritium and helium in the breeding-blanket-relevant liquid lithium–lead eutectic alloy: *ab-initio* molecular dynamics simulations

**Beatriz G del Rio**[1,*], **Joël Martín Dalmas**[1], **Nonia Vaquero-Sabater**[2,3], **David J González**[1] and **Luis E González**[1]

[1] Departamento de Física Teórica, Universidad de Valladolid, 47011 Valladolid, Spain
[2] Donostia International Physics Center, 20018 San Sebastian, Spain
[3] Departamento de Polímeros y Materiales Avanzados: Física, Química y Tecnología. Universidad del País Vasco, 20080 San Sebastián, Spain
[*] Author to whom any correspondence should be addressed.

**E-mail:** beatriz.gonzalez.rio@uva.es

**Keywords:** breeding blanket, fusion reactors, liquid lithium–lead eutectic, tritium, helium bubbles

## Abstract

The lead-rich liquid lithium–lead eutectic alloy, $Li_{17}Pb_{83}$, is one of the candidates to be used in breeding blanket modules of future fusion reactors where tritium breeding is essential to provide the necessary fuel for fusion. It has several properties that favour its use, such as the breeding capacity of Li, the neutron multiplication capacity of Pb, the ease of circulation for off-site tritium recovery, and the capability to, at least partly, refrigerate the system. It is therefore important to understand the properties of the tritium generated in the breeding reactions, and its effects on the hosting liquid. The same applies to helium nuclei that are generated in a 1:1 ratio to tritium in the breeding reactions. We have performed first principles molecular dynamics simulations to study the structural changes observed in liquid $Li_{17}Pb_{83}$ when tritium or helium is added. In one set of simulations we have made calculations for several amounts of tritium, with molar concentrations ranging from 0.20 to 0.03, without any He atoms. In the other set of simulations we have included helium atoms with molar concentration 0.11, and no tritium. Tritium atoms are found to bind preferentially with Li, modifying substantially the Li–Li correlation functions. We also observe the presence of long-lasting di-tritium molecules when tritium concentration is not too low, which also tend to bind to Li atoms. The velocity autocorrelation functions of tritium, Li and Pb are evaluated, and analysed in order to obtain the corresponding vibrational properties of the different species. Helium atoms tend to aggregate together forming a cluster whose characteristics are reported, together with the correlation functions of He atoms with Li and Pb. The motion of He atoms within this cluster is found to be sub-diffusive, while an estimate of He mobility outside the aggregate is also given.

## 1. Introduction

In the pursuit of reliable, secure, and environmentally sustainable energy production, fusion reactors have been regarded for several decades as highly promising systems [1]. Although the physical principle underlying controlled nuclear fusion is conceptually straightforward, its practical realization involves substantial technological challenges. These challenges arise, on one hand, from the complex behaviour of high-temperature high-density plasmas and, on the other, from the demanding requirements placed on materials that must withstand extreme operational conditions, including intense heat loads and radiation. Among the various fusion reactions under consideration, the deuterium–tritium (D–T) reaction is regarded as the most favourable for controlled energy production [2]. This reaction produces alpha

particles ($^4$He) and neutrons, the latter carrying the majority of the released energy in the form of kinetic energy. The naturally occurring inventory of tritium is negligibly small because it is a radioactive isotope, that decays through $\beta$ emission to $^3$He, with a relatively short half-life of 12.32 years [3]. Consequently, the required tritium must be produced artificially. Tritium breeding in future fusion reactors will proceed [4] through neutron-induced fission of lithium isotopes, primarily $^6$Li (n+$^6$Li $\rightarrow$ T + $^4$He) and to a lesser extent $^7$Li (n+$^7$Li $\rightarrow$ T + $^4$He + n′) to ensure tritium self-sufficiency. The Li-containing material (blanket) surrounds the plasma chamber and serves also [5] to shield the fusion-generated neutrons and to extract their energy, which is ultimately intended to be converted into electrical power in future reactor designs, such as the DEMO (demonstration power plant) concept [6]. One of the most promising blanket materials currently under consideration is the lead-rich liquid lithium–lead eutectic alloy (LLE), $Li_{17}Pb_{83}$ [7]. This material offers several advantages over alternative breeders, including neutron multiplication capabilities associated with specific lead isotopes, ease of circulation due to its liquid state, partial contribution to the cooling function owing to its high thermal conductivity, a moderately low melting point, reduced chemical reactivity as compared to pure lithium, and a low solubility of tritium in the alloy, which facilitates its extraction.

The comprehensive analysis of tritium behaviour throughout the entire fuel cycle (storage, plasma injection, breeding, transport, extraction) requires the knowledge of numerous state-dependent thermophysical properties of the liquid alloy and its interaction with both tritium and helium (see, for example, [8]). Experimental observations [9] suggest that helium atoms may aggregate and form bubbles, which can themselves act as trapping sites for tritium, alter the thermal transport properties of the blanket, or modify the magnitude and character of magnetohydrodynamic effects. While some thermophysical properties, such as the density or the surface tension, are readily available [10, 11], others present substantial uncertainty due to the intrinsic challenges of experimental measurement, which lead to significant discrepancies among reported values. Notable examples include the state-dependent solubility of tritium (see [12] and references therein), its diffusivity [13–16], and the same magnitudes for helium. In the latter case, there is no experimental information about the solubility (other that it is very small but not zero) and only some empirical estimations [17] exist. The diffusivity of atomic He, and basic characteristics of the potential He bubbles, such as their density, internal pressure, or mobility, are essentially unknown from an experimental standpoint.

Molecular dynamics (MD) simulations provide an effective means of determining these properties, as they circumvent the experimental limitations. In the case of tritium dissolved in the LLE alloy we are only aware of one MD study [18], that was carried out through *ab initio* techniques at 900 K, using 6 Li atoms, 30 Pb atoms and 1 hydrogen atom (instead of tritium). The total simulation time was 1 ps, and the authors focused on the analysis of the charge associated to the H atom (using the Mulliken population approach) depending on its distance to a Li atom. They also considered how the H atom moved attaching to and detaching from Li atoms. However, due to the limited number of atoms and the short simulation time, important magnitudes such as the diffusion coefficient could not be computed. He dissolved in the LLE through MD techniques has received some more attention in the literature, but in this case all of the studies have modelled the interactions through effective interatomic potentials and no first principles simulations have been conducted to date. Fraile and Polcar [19] studied systems made up of up to 1.15 million particles, where Li–Li, Li–Pb and Pb–Pb interactions were modelled through an embedded atom many-body potential, whereas He–He, He–Li and He–Pb interactions were modelled through Lennard-Jones potentials. They obtained a number of properties of He bubbles of several sizes, but they also discussed that those properties can change upon variation of the parameters used in the model potential. Alvarez-Galera *et al* [20] applied perturbative techniques to compute the free energy of insertion of one He atom in the liquid LLE using MD simulations at constant pressure and temperature, and obtained a value of the Henry's constant that characterizes the He solubility. The number of atoms of the liquid metal was 1024 and a total time of 35 ns was simulated. The interactions among liquid metal atoms were modelled again through an embedded atom model (although not the same one as that of Fraile and Polcar) while the interactions of He with other atoms were taken from in-vacuum calculations of the potential energy as a function of separation between the atoms. Al-Awad *et al* [21] performed stochastic computer experiments to study the thermodynamic irreversibility of He nanobubbles in the liquid LLE, employing the same potentials as Alvarez-Galera *et al*.

Effective interatomic potentials, whether pairwise or many-body in nature, are invariably subject to questions regarding their transferability from the conditions under which they were constructed to the distinct environments where they are subsequently applied. For example, one may ask whether the interaction between two helium atoms determined in vacuum, remains unchanged in the presence of a nearby lithium atom, or whether the interaction between two lithium atoms in the alloy is altered when tritium is present in the local configuration. A prominent contemporary strategy for describing

interatomic interactions relies on machine-learning techniques, such as neural-network potentials (see, for instance, [22]). These approaches can achieve a level of accuracy comparable to first-principles calculations while requiring only a fraction of their computational cost. As a result, they enable the simulation of complex systems using large samples and long trajectories that would be impractical with fully first-principles methods. Nevertheless, first-principles simulations remain essential to generate the training datasets, particularly atomic forces, required for constructing reliable machine-learned potentials. This is precisely what we provide in the present work. We have performed *ab initio* simulations for two classes of three-component systems: liquid LLE alloys with dissolved tritium, and liquid LLE alloys with dissolved helium. Beyond supplying the necessary datasets for future development of machine-learning potentials, these simulations allow an accurate characterization of the structural properties of the systems, as captured by their pair distribution functions and/or density profiles, as well as the determination of some dynamic properties such as diffusivities or vibrational spectra of the species examined in each case. In the case of tritium dissolved in the liquid LLE alloy we have increased substantially the size of the simulated sample and the total simulation time as compared to those of Masuyama *et al* [18], and have discussed the dependence of the obtained properties on tritium concentration within the limits imposed by the cost of first principles simulations. In the case of He dissolved in the liquid LLE alloy the present study is the first one carried out *ab initio* as far as we are aware.

Section 2 describes the computational methodology employed, together with the details of the simulated samples and the thermodynamic states considered. The results for the structural and dynamical properties of the systems containing tritium are presented in section 3 and those of the helium containing system in section 4. Finally, section 5 provides a summary of the work and outlines the main conclusions.

## 2. Computational details

We have carried out *ab initio* MD (AIMD) simulations of LLEs containing either dissolved tritium (LLE+T) or helium (LLE+He), specifically systems of the form $T_x(Li_{17}Pb_{83})_{1-x}$ and $He_x(Li_{17}Pb_{83})_{1-x}$. For tritium, molar concentrations $x$ ranging from 0.20 to 0.03 were considered, while for helium a concentration of $x = 0.111$ was examined. These concentrations are significantly higher than those expected in an operational blanket (in the range of less than 1 appm, i.e. $10^{-6}$ [23]), but are required to achieve sufficient statistical accuracy given the small number of solvent atoms in AIMD simulations. More dilute systems would demand prohibitively large samples due to the computational cost of *ab initio* methods and their study must be postponed until appropriate machine-learned potentials have been constructed.

Table 1 summarizes the characteristics of the simulated systems and the thermodynamic states explored. Each sample contains $N_{Li} = 43$ lithium atoms, $N_{Pb} = 213$ lead atoms, and a number of dissolved tritium or helium atoms, $N_T$ and $N_{He}$, respectively.

The simulations were performed within the framework of density functional theory [24, 25], using the VASP package [26]. The PBE exchange–correlation functional [27] and PAW potentials [28] were employed, with one valence electron for T and Li, two for He, and four for Pb. A plane-wave energy cutoff of 400 eV was used. The integration timestep was set to 1 fs for the tritium-containing systems and 2.5 fs for the helium-containing system. The number of equilibrium configurations generated after appropriate thermalization ranged from 15 000 to 30 000 for the LLE+T systems and was 10 000 for the LLE+He system, spanning total simulation times between 15 and 30 ps. The temperature was set in all cases to 775 K, as in previous studies of the pure LLE alloy [29, 30]. The number densities of all of the systems were adjusted to obtain a pressure of few kbars, but for the system richest in tritium we have additionally considered a higher density (and consequently a higher pressure, around 150 kbar) in order to analyse the density (or pressure) dependence of the magnitudes studied.

## 3. Results: tritium dissolved in the liquid LLE.

The structure of the LLE+T systems, composed of $N_i$ particles of species $i$ and a total number of particles $N = \sum_i N_i$, is reported in subsection 3.1 and has been characterized in terms of the pair correlation functions, $g_{ij}(r)$, and the corresponding pair distribution functions, defined as

$$G_{ij}(r) = 4\pi r^2 \rho c_j g_{ij}(r), \tag{1}$$

**Table 1.** Sample details and thermodynamic states studied in this work. $N_{\mathrm{Li}}$ and $N_{\mathrm{Pb}}$ are the number of Li and Pb atoms in the samples, $N_{\mathrm{T}}$ and $N_{\mathrm{He}}$ are the number of tritium and helium atoms respectively, $x$ is the molar concentration of the dissolved species. The temperature $T$ is given in K, the number density, $\rho$, in atoms per Å$^3$ and the pressure, $P$, in kbar.

| $N_{\mathrm{Li}}$ | $N_{\mathrm{Pb}}$ | $N_{\mathrm{T}}$ | $N_{\mathrm{He}}$ | $x$ | $T$ | $\rho$ | $P$ |
|---|---|---|---|---|---|---|---|
| 43 | 213 | 64 | 0 | 0.200 | 775 | 0.050 37 | 150 |
| 43 | 213 | 64 | 0 | 0.200 | 775 | 0.038 78 | 18 |
| 43 | 213 | 32 | 0 | 0.111 | 775 | 0.035 74 | 13 |
| 43 | 213 | 16 | 0 | 0.059 | 775 | 0.033 46 | 7 |
| 43 | 213 | 8 | 0 | 0.030 | 775 | 0.032 48 | 6 |
| 43 | 213 | 0 | 32 | 0.111 | 775 | 0.031 07 | $\approx 0$ |

where $c_j = N_j/N$ denotes the concentration of species $j$. The function $G_{ij}(r)$ represents the radial distribution of particles of type $j$ around a reference particle of type $i$. Its integral,

$$N_{ij}(R) = \int_0^R \mathrm{d}r\, G_{ij}(r)\,, \tag{2}$$

gives the number of neighbours of species $j$ within a distance $R$ from a particle of species $i$.

Although $g_{ij}(r)$ and $G_{ij}(r)$ encode the same structural information, they exhibit distinct properties that may render one or the other more convenient depending on the context. Note that the pair correlation functions are symmetric under the interchange of indices $i$ and $j$, whereas the pair distribution functions are not, due to the explicit dependence on the concentration factor $c_j$.

We also introduce the total distribution function around a particle of species $i$, defined as

$$G_i(r) = \sum_j G_{ij}(r)\,, \tag{3}$$

which describes the radial distribution of particles, irrespective of species, around an $i$-type particle. The corresponding integrated quantity, $N_i(R)$, yields the total number of neighbours within a distance $R$ from the reference particle. These total distribution functions are particularly suitable for analysing the coordination structure around a particle of species $i$. The position of the first minimum of $G_i(r)$, denoted $R_i^{\min}$, defines the spatial extent of the first coordination shell. The value $n_i = N_i(R_i^{\min})$ gives the total number of first neighbours (total coordination number), while $n_{ij} = N_{ij}(R_i^{\min})$ provides the partial coordination number associated with the first neighbours of species $j$ around the $i$-type particle.

Note that for an $n$-component system there are $n$ different total distribution functions, $n^2$ different pair distribution functions, and $n(n+1)/2$ different pair correlation functions.

The single-particle dynamics are usually characterized by the mean squared displacements, $\delta r_i^2(t)$, the velocity autocorrelation functions, $Z_i(t)$, and the corresponding power spectra, $\hat{Z}_i(\omega)$, defined as

$$\delta r_i^2(t) = \left\langle \left| \vec{r}_i(t+t_0) - \vec{r}_i(t_0) \right|^2 \right\rangle, \tag{4}$$

$$Z_i(t) = \frac{\langle \vec{v}_i(t+t_0) \cdot \vec{v}_i(t_0) \rangle}{\langle \vec{v}_i \cdot \vec{v}_i \rangle}, \tag{5}$$

where $\vec{r}_i$ and $\vec{v}_i$ denote the position and velocity of a particle of species $i$, respectively. The angular brackets indicate averages over particles of the same species and over different time origins $t_0$. The power spectrum is given by

$$\hat{Z}_i(\omega) = \int_0^\infty \mathrm{d}t Z_i(t) \exp(-\mathrm{i}\omega t)\,. \tag{6}$$

At short times, the mean squared displacement exhibits a ballistic regime and increases quadratically with time, $\delta r_i^2(t) \sim \langle \vec{v}_i \cdot \vec{v}_i \rangle t^2 = (k_{\mathrm{B}}T/m_i)\, t^2$, where $k_{\mathrm{B}}$ is the Boltzmann constant and $m_i$ is the mass of particles of species $i$. At long times, after many collisions have occurred, the system reaches a diffusive regime in which the mean squared displacement grows linearly with time. The self-diffusion coefficient is then obtained from the long-time slope as $D_i = \lim_{t\to\infty} \frac{1}{6}\, \mathrm{d}[\delta r_i^2(t)]/\mathrm{d}t$.

The velocity autocorrelation function quantifies the decay of memory of the initial particle velocity due to interactions with surrounding particles. Its Fourier transform, the power spectrum, highlights the characteristic vibrational frequencies of the atomic motion as distinct peaks. In addition, the self-diffusion coefficient can be determined from the zero-frequency limit of the power spectrum according to $D_i = (k_{\mathrm{B}}T/m_i)\, \hat{Z}_i(\omega = 0)$.

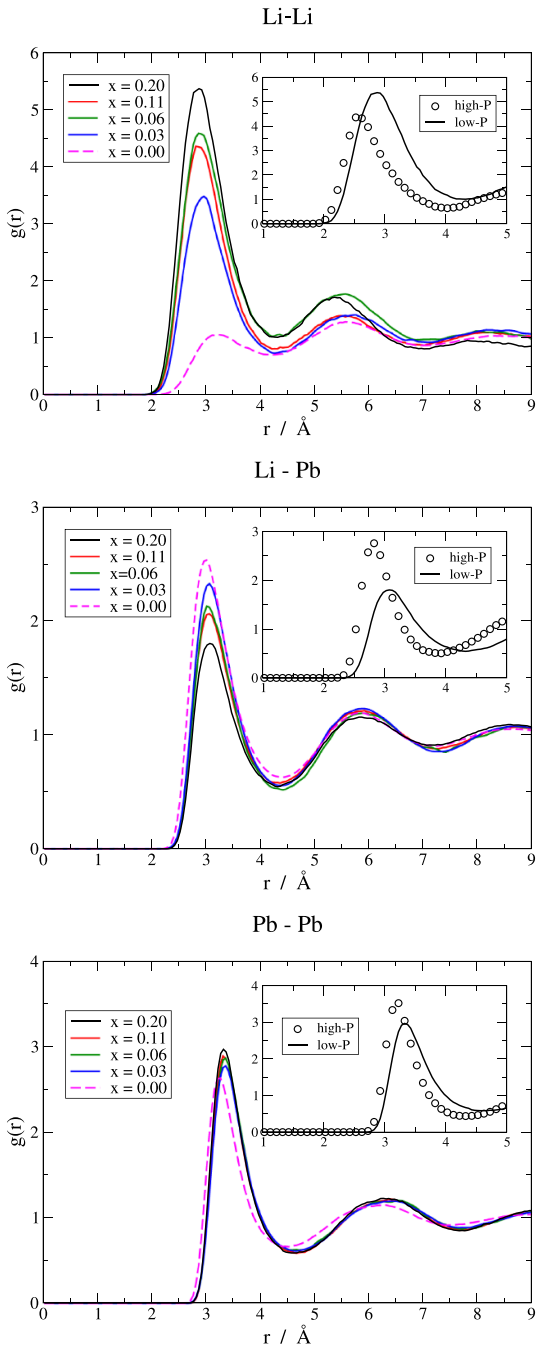


**Figure 1.** Li–Li, Li–Pb and Pb–Pb pair correlation functions for different tritium concentrations. The insets show the results for $x = 0.20$ at high and low pressures. The data for the pure LLE alloy are from [29].

### 3.1. Structure

The pair correlation functions involving only Li and Pb atoms are shown in figure 1, and are compared with the corresponding $g_{ij}(r)$ of the tritium-free alloy ($x = 0$) [29]. The Pb–Pb pair correlation functions are found to be only weakly affected by the presence of T atoms. In contrast, those correlations involving Li atoms exhibit pronounced modifications upon tritium incorporation. In particular, the Li–Pb correlations show a partial depletion in the region of the first peak, while the Li–Li correlations increase markedly when tritium is added. This behaviour indicates that Li atoms are displaced from the vicinity of Pb atoms and preferentially cluster together, with T atoms effectively acting as a binding agent between them. The main effect of pressurization is a displacement of the typical distances towards smaller values.

We next consider the structural functions where tritium atoms are involved. In the case of T–T and T–Li functions we show in figure 2 the pair distribution functions, $G_{\mathrm{T,T}}(r)$ and $G_{\mathrm{T,Li}}(r)$, because of the very high amplitude of the first peak of the corresponding $g_{i,j}(r)$. The $r^2$ factor in the pair distribution

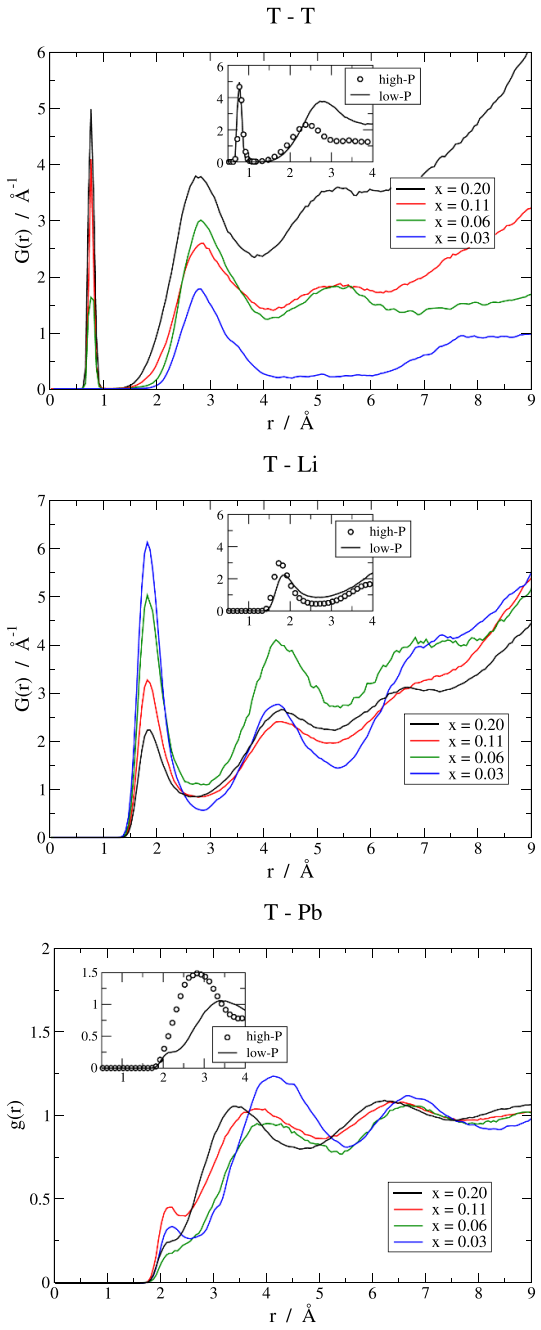


**Figure 2.** Pair distribution functions $G_{T,T}(r)$ and $G_{T,Li}(r)$, together with the pair correlation function $g_{T,Pb}(r)$ for different tritium concentrations. The insets show the results for $x = 0.20$ at high and low pressures.

functions render this first peak low enough to fit in the scale of the graphs. The results for $g_{T,Pb}(r)$ are also reported in figure 2. The presence of a sharp and intense peak in the T–T correlations at a distance of approximately 0.75 Å indicates the formation of $T_2$ molecules in systems with sufficiently high tritium molar concentration. These molecules account for roughly two thirds of the total number of T atoms and coexist with the remaining fraction of tritium in atomic form. Furthermore, they are stable over time scales long enough to leave an unambiguous signature in the structural correlation functions. For concentrations $x \leqslant 0.03$, no molecular species are observed during the simulation runs. The resulting interpretation is that molecular formation occurs whenever the tritium concentration is high enough to provide a non-negligible probability for two T atoms to encounter each other and bind. This finding is particularly noteworthy, as it is commonly assumed that hydrogen dissolved in metals exists exclusively in atomic form. Molecular dissociation is generally attributed to the interaction of hydrogen molecules with the metallic surface, followed by diffusion of the resulting hydrogen atoms into the bulk, which prevents recombination. In contrast, the present results demonstrate that $T_2$ molecules formed inside the bulk can indeed persist in the metallic environment, with lifetimes of at least several picoseconds,

i.e. within the time window explored by our simulations. As will be shown below, the existence of these molecules leaves a clear imprint not only on the structural properties but also on the dynamical behaviour of the system, manifesting itself as a characteristic vibrational frequency in the motion of T atoms. The observation of molecular hydrogen coexisting with its atomic form within a liquid metal during a simulation run is in fact not new. It has been detected previously in several systems, such as Pb–Bi alloys [31], pure Li [32], or Li–Sn alloys [33], when the total amount of hydrogen is high enough. In order not to disrupt the presentation of the main results, we defer to the appendix a brief discussion about the physical mechanisms that could be behind the lack of dissociation of these molecular units in the particular case of the Li–Pb alloy considered here. The main idea is that once the molecule is formed inside the bulk liquid, Pb does not favour dissociation, while a single Li atom cannot break the molecular strong covalent bond without the cooperation of other Li atoms.

The first peak observed in the T–Li structural correlation function is also very intense, but significantly broader. This feature rules out the formation of stable LiT molecular species, while nevertheless indicating a strong attractive interaction between Li and T atoms. In contrast, the interaction between T and Pb atoms appears to be very weak. Indeed, the $g_{\mathrm{T,Pb}}(r)$ function closely resembles a uniform distribution of Pb atoms beyond the excluded-volume region imposed by the atomic sizes. The effect of pressure on these structural functions amounts again mainly to a reduction of the characteristic distances, except of course the interatomic distance in $T_2$ molecules.

The existence of long-lived tritium molecules makes more convenient to treat the system as a four-component system, with Li, Pb, T in atomic form (we will denote it as $T_{\mathrm{atom}}$) and $T_2$ molecules. Within this interpretation, we plot in figure 3 the $g_{i,j}(r)$ functions for $i = \mathrm{T_{atom}}, \mathrm{T_2}$. The results show that Li, tritium atoms and tritium molecules are strongly correlated among themselves, while the tritium-Pb interaction is again very weak, irrespective of considering tritium in atomic or in molecular form.

We end up the discussion about structure by analysing the coordination structure of the different atoms and molecules present in the liquid. To this end we compute the total distribution functions, $G_i(r)$, presented in figure 4, identify the $R_i^{\mathrm{min}}$, and perform the corresponding integrals, as explained above, to obtain the $n_i$ and $n_{ij}$ coordination numbers. These are reported in table 2.

The first coordination shell of Li is found to be formed almost exclusively by atomic tritium, whereas the second coordination shell is basically the one that corresponded to the pure alloy without tritium dissolved, meaning it is formed by Li and Pb atoms. In the case of Pb the first coordination shell is that of the underlying alloy, irrespective of tritium concentration. Around a tritium in atomic form we observe a first shell made up mostly of Li atoms, with a small contribution from Pb atoms too. A second coordination shell, mostly formed by other tritium atoms, can hardly be distinguished for high tritium concentration. Finally the total distribution function around a tritium molecule at low pressures, when these molecules exist, is very diffuse and it is not possible to discern any shell structure. Only upon pressure increase a first coordination shell can be observed, with a maximum around 1.98 Å and a very shallow minimum around 2.20 Å that enables the computation of $T_2$ coordination numbers, although with a relatively high uncertainty. In any case, the position of the first peak of the pair correlation function $g_{\mathrm{T_2,Li}}(r)$ indicates, for each tritium concentration (and pressure), the most probable distance between tritium molecules and Li atoms, $r^{\mathrm{max}}_{\mathrm{T_2-Li}}$. These distances are reported also in table 2.

The main features reported in table 2 for Li, Pb and $T_{\mathrm{atom}}$ are also illustrated in figure 5. In this figure, we additionally indicate the position of the first maximum of the total pair distribution functions $G_i(r)$, which serves as a representative measure of the location of the first coordination shell. The positions of this first maximum coincide for lithium and tritium atoms, and are basically independent of T content, whereas the corresponding maximum for lead atoms is located at a significantly larger distance.

It should be noted that the average number of tritium atoms coordinated to a lithium atom, $n_{\mathrm{Li-T_{atom}}}$, is strongly influenced by the total tritium content of the simulation cell, which becomes significantly smaller than the number of lithium atoms as the concentration $x$ decreases (see table 1). Consequently, at low values of $x$, the most probable value of $n_{\mathrm{Li-T_{atom}}}$ is zero, and Li atoms that are not coordinated with T are instead coordinated with Pb and other Li atoms. This observation indicates that two distinct populations of lithium atoms coexist in the liquid: those coordinated with tritium and those that are not, whose local environments and properties may therefore differ. Figure 6 presents the Li–Li pair correlation functions for the system with $x = 0.03$, distinguishing between lithium atoms coordinated with tritium (denoted as $\mathrm{Li_a}$) and those not coordinated with tritium (denoted as $\mathrm{Li_b}$). The results clearly reveal markedly different behaviours for the two populations. In particular, the $g_{\mathrm{Li_a,Li_a}}(r)$ function exhibits a pronounced first peak of very high amplitude, whereas those correlation functions that involve $\mathrm{Li_b}$ atoms resemble more closely the Li–Li pair correlation function of the underlying pure LLE alloy, shown in figure 1, with a first maximum of amplitude close to unity. Furthermore, the average number of T neighbours associated to a tritium-coordinated Li atom is calculated to be $n_{\mathrm{Li_a-T}} = 1.16$.

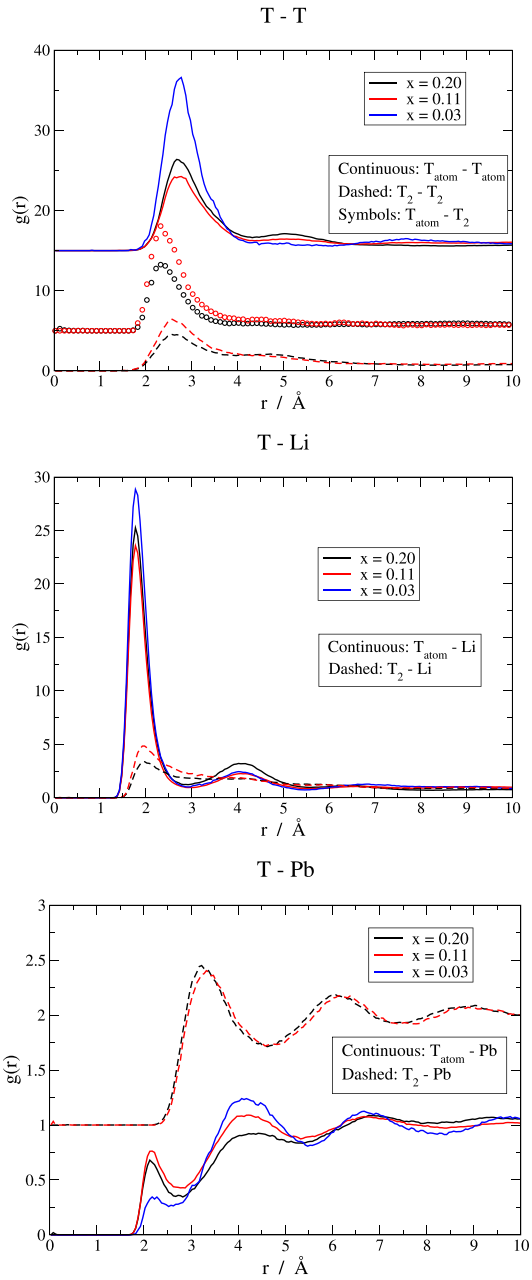


**Figure 3.** Pair correlation functions $g_{i,j}(r)$ within the four-component treatment, that involve tritium in atomic or molecular form. Some of the functions have been shifted upwards for better visualization.

In summary, our main conclusions regarding the first coordination shells are that tritium atoms are coordinated with roughly three Li atoms for all of the tritium concentrations investigated at low pressure, with this coordination number reducing to roughly two Li atoms at high pressure, while Li atoms coordinated with T exhibit roughly one tritium neighbour across all LLE+T systems studied.

### 3.2. Single-particle dynamics

We have evaluated the velocity autocorrelation functions and the power spectra of the different species for the LLE+T systems. As an example we illustrate in figure 7 the corresponding functions for Li, Pb and T in the system with $x = 0.11$.

The overall behaviour of the $Z_i(t)$ follows the general trends of dense liquid systems, exhibiting a backscattering minimum followed by damped oscillations that decay to zero, with the location of the backscattering minima reflecting the masses of the particles. In the case of T an additional high-frequency small-amplitude component is clearly visible in the velocity autocorrelation function, which can be attributed to the oscillations of the interatomic separation during the evolution of $T_2$ molecules. Consistently, the power spectrum $\hat{Z}_T(\omega)$ displays a distinct high-frequency peak, located at $\approx 407\,\mathrm{ps}^{-1}$,

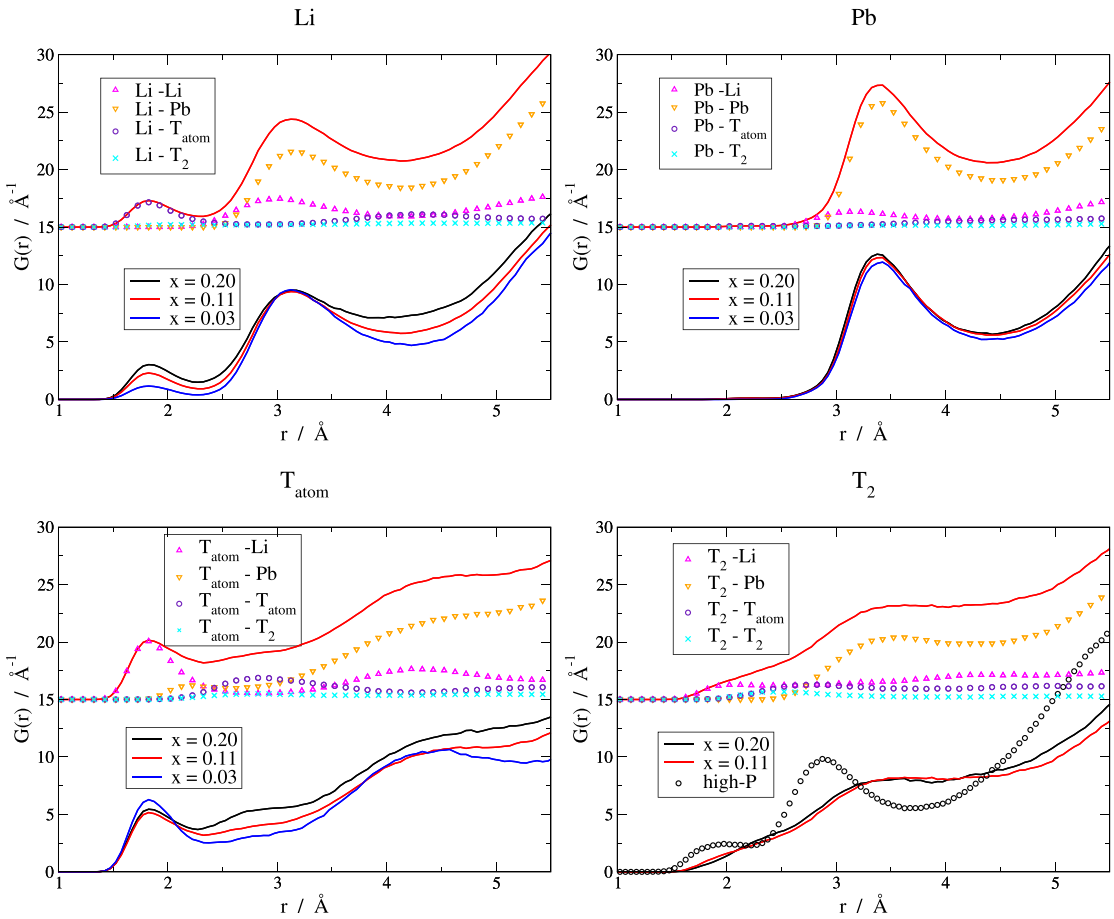


**Figure 4.** Total correlation functions for several tritium concentrations and its decomposition for $x = 0.11$. In the case of the $G_{T_2}(r)$ we also include the results corresponding to $x = 0.20$ and high pressure.

which is absent in the power spectra of Li and Pb atoms. In order to verify the molecular origin of this feature we have monitored the time-dependent distance between T atoms in the molecules present in the system, and obtained its Fourier Transform. This analysis reveals a peak of frequency $\approx 415\,\mathrm{ps}^{-1}$, indicated by a vertical arrow in 7, in close agreement with the high frequency maximum observed in $\hat{Z}_T(\omega)$. It should be noted that this frequency is somewhat smaller than the stretching frequency of the free $T_2$ molecule ($\approx 469\,\mathrm{ps}^{-1}$ [34]), due to the effect of its interaction with the liquid alloy where it is dissolved, and in particular with the Li atoms coordinated with the molecule. We have indeed observed a direct relationship between the stretching frequency and $r^{\max}_{T_2-Li}$, reported in table 2, with the frequency reducing to $\approx 367\,\mathrm{ps}^{-1}$ for the high-pressure system.

By comparing the power spectra at different concentrations we can analyse if the amount of T and the pressure have any influence on the characteristic frequencies of atomic motion, identified through the peaks in the $\hat{Z}_i(\omega)$. Figure 8 shows such comparison for $x = 0.03$ and 0.11 at low pressure and for the high-pressure $x = 0.20$ case, with the comparison restricted to frequencies lower than $200\,\mathrm{ps}^{-1}$. We observe quite similar frequencies at both values of $x$ and low pressure, although the corresponding amplitudes do differ, thus suggesting little dependence of these characteristic frequencies on the tritium content. We also observe that tritium atoms show two distinct characteristic frequencies, a higher one, expected due to the lower atomic mass of T atoms, and a lower one coincident with the typical frequency of Li atoms. The existence of this similar frequency in the spectra of Li and T underlines once more their mutual strong interaction. Pressurization of the system makes the characteristic frequencies shift towards larger values (excepting the stretching $T_2$ one, that becomes smaller as commented previously), but still maintaining the existence of a common component for Li and T.

We have not been able to evaluate reliably the diffusion coefficients of T in our systems. In the case of the most diluted system, $x = 0.03$, there are only 8 tritium atoms, and the statistical uncertainties in the evaluation of the mean square displacements are rather large. For instance, the results depend strongly upon the selected time interval for the evaluation of the $\delta r^2(t)$, and a computation of this function particle by particle (instead of just their average) shows very large differences between each other.

**Table 2.** Total and partial coordination numbers of the different species present in the LLE+T systems. The extent of the first coordination shell, $R_i^{\min}$, and the most probable distance between tritium molecules and Li atoms, $r^{\max}_{T_2-Li}$, are given in Å. For $x = 0.03$ no $T_2$ molecules exist. Dashes indicate that the magnitudes are not defined because there is no minimum in the total distribution function.

| $x$ | 0.03 | 0.06 | 0.11 | 0.20 | 0.20 high-P |
|---|---|---|---|---|---|
| $R_{Li}^{\min}$ | 2.28 | 2.28 | 2.30 | 2.26 | 2.17 |
| $n_{LiLi}$ | 0.01 | 0.02 | 0.02 | 0.02 | 0.03 |
| $n_{LiPb}$ | 0.00 | 0.00 | 0.00 | 0.00 | 0.00 |
| $n_{LiT_{atom}}$ | 0.56 | 0.83 | 1.06 | 1.33 | 1.30 |
| $n_{LiT_2}$ | | 0.03 | 0.11 | 0.22 | 0.37 |
| $n_{Li}$ | 0.57 | 0.88 | 1.18 | 1.57 | 1.70 |
| $R_{Pb}^{\min}$ | 4.38 | 4.33 | 4.38 | 4.43 | 4.09 |
| $n_{PbLi}$ | 1.74 | 1.54 | 1.61 | 1.47 | 1.71 |
| $n_{PbPb}$ | 9.66 | 9.66 | 9.81 | 9.99 | 10.56 |
| $n_{PbT_{atom}}$ | 0.26 | 0.27 | 0.60 | 0.62 | 0.87 |
| $n_{PbT_2}$ | | 0.06 | 0.24 | 0.76 | 0.88 |
| $n_{Pb}$ | 11.66 | 11.53 | 12.26 | 12.84 | 14.02 |
| $R_{T_{atom}}^{\min}$ | 2.38 | 2.33 | 2.33 | 2.28 | 1.99 |
| $n_{T_{atom}Li}$ | 3.18 | 3.06 | 2.52 | 2.62 | 2.11 |
| $n_{T_{atom}Pb}$ | 0.20 | 0.15 | 0.42 | 0.31 | 0.08 |
| $n_{T_{atom}T_{atom}}$ | 0.12 | 0.12 | 0.10 | 0.09 | 0.05 |
| $n_{T_{atom}T_2}$ | | 0.03 | 0.06 | 0.10 | 0.06 |
| $n_{T_{atom}}$ | 3.50 | 3.36 | 3.10 | 3.12 | 2.30 |
| $r^{\max}_{T_2-Li}$ | | 2.18 | 1.95 | 1.98 | 1.76 |
| $R_{T_2}^{\min}$ | | — | — | — | 2.20 |
| $n_{T_2Li}$ | | — | — | — | 0.80 |
| $n_{T_2Pb}$ | | — | — | — | 0.00 |
| $n_{T_2T_{atom}}$ | | — | — | — | 0.17 |
| $n_{T_2T_2}$ | | — | — | — | 0.31 |
| $n_{T_2}$ | | — | — | — | 1.28 |

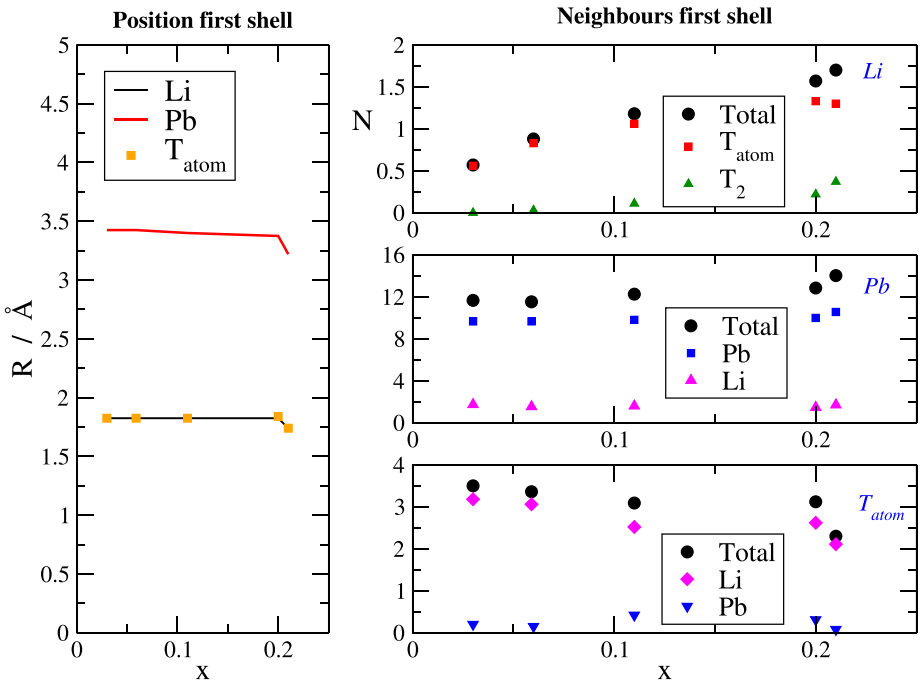


**Figure 5.** Main characteristics of the first coordination shells of Li, Pb and atomic T. The data plotted at $x = 0.21$ correspond to the high pressure values of $x = 0.20$.

This means that much longer simulation times, not affordable within the AIMD scheme, would be required for a reliable determination of this property. With increasing tritium content the problem now lies in the coexistence of tritium in atomic and molecular form in the system. Molecules are expected to

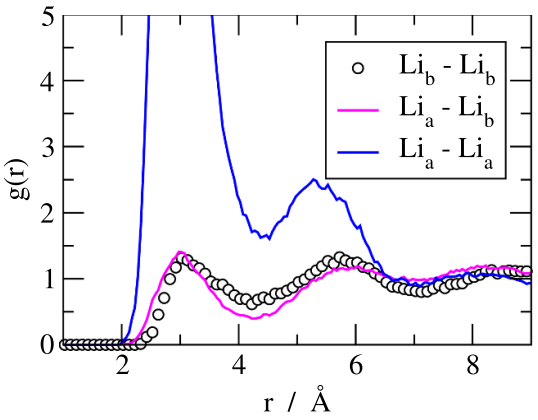


**Figure 6.** Li–Li pair correlation functions for the different types of Li atoms according to their coordination with tritium for the LLE+T system with $x = 0.03$.

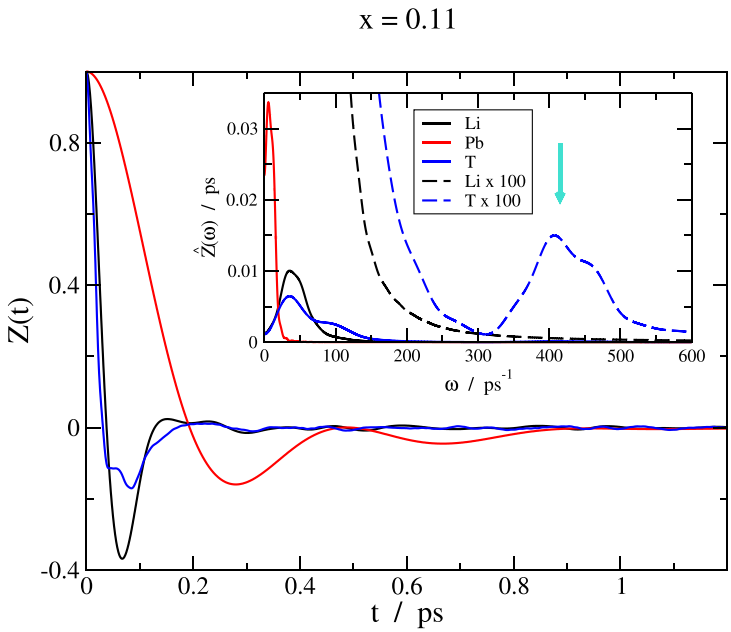


**Figure 7.** Velocity autocorrelation functions (main panel) and power spectra (inset) of Li, Pb and T for the LLE+T system with $x = 0.11$. The arrow indicates the frequency of the oscillations in the interatomic distance of the $T_2$ molecules.

diffuse more slowly than atoms and therefore a straight application of the definition of $\delta r^2(t)$ as an average over all of the tritium atoms would lead to results that are not truly representative of atomic tritium diffusion.

Consequently, we were forced to defer the evaluation of this important dynamic property to a later stage when machine learned interatomic potentials based on the present simulations are constructed, and much longer simulation times become affordable.

## 4. Results: Helium dissolved in the liquid LLE.

The He atoms of the sample were initially placed at random positions within the simulation cell, and the LLE+He sample was allowed to evolve at constant temperature. After the initial equilibration stage the atomic positions and velocities were collected over 10 000 configurations, and subsequently employed to investigate the structural and dynamic properties of the system. During the equilibrium run several distinct groups of helium atoms were observed to form. Two He atoms were considered to be connected within a group if their relative distance was smaller that twice the He van der Waals radius, 1.40 Å. The

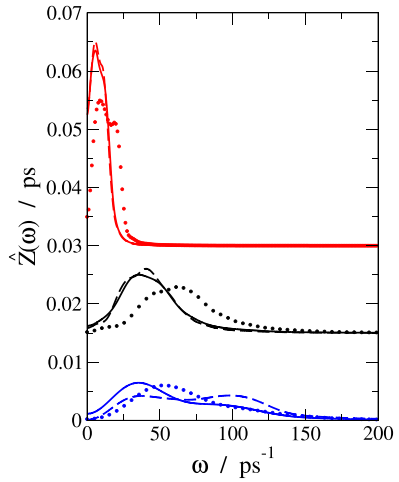


**Figure 8.** Power spectra of Li (black), Pb (red) and T (blue) for the LLE+T systems with $x = 0.11$ (continuous lines) and 0.03 (dashed lines) and $x = 0.20$ at high pressure (circles).

**Table 3.** Stability of the groups with different number of He atoms during the 25 ps long simulation run.

| Size of the group | 1 | 2 | 3 | 4 | 5 | ⋯ | 21 | ⋯ | 26 | ⋯ |
|---|---|---|---|---|---|---|---|---|---|---|
| Time of stability (ps) | 7 | 25 | 12.5 | 11.25 | 3.75 | | 3.75 | | 12.5 | |

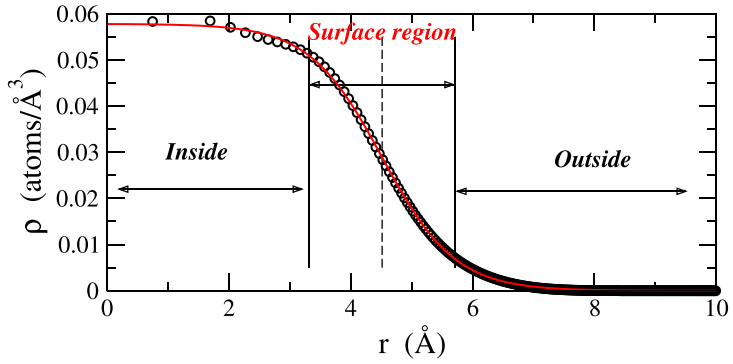


**Figure 9.** Radial density profile of the 26-atom He cluster. Black circles: simulation results, red line: fit to a tanh profile.

groups formed include isolated atoms (i.e. with no He neighbours), dimers, trimers, and larger aggregates up to a cluster containing 27 atoms. These groups remain stable for finite periods of time, as summarized in table 3, after which they typically disappear by merging with another cluster. The 26-atom cluster exhibits a rather long lifetime once formed, and has therefore been selected for detailed analysis.

### 4.1. Structure

Although the instantaneous shape of the 26-atom cluster is not perfectly spherical, its structural properties can still be characterized by performing angular averages relative to the instantaneous centre of mass of the aggregate. The resulting mean radial density profile of the helium atoms is presented in figure 9. The profile, $\rho(r)$, has been obtained counting the number of atoms enclosed in spherical shells whose widths have been selected to have a similar volume in order to alleviate statistical inaccuracies near the centre of mass. The form observed is rather standard, decaying monotonically from the centre, through the interfacial region, and into the liquid alloy. The shape has been fitted to a tanh profile,

$$\rho(r) = \frac{\rho_0}{2}\left[1 + \tanh\left(\frac{R-r}{w}\right)\right], \tag{7}$$

from which we obtain an internal density $\rho_0 = 0.0578\,\text{Å}^{-3}$, a cluster radius $R = 4.52\,\text{Å}$, and a surface width $w = 1.19\,\text{Å}$ .

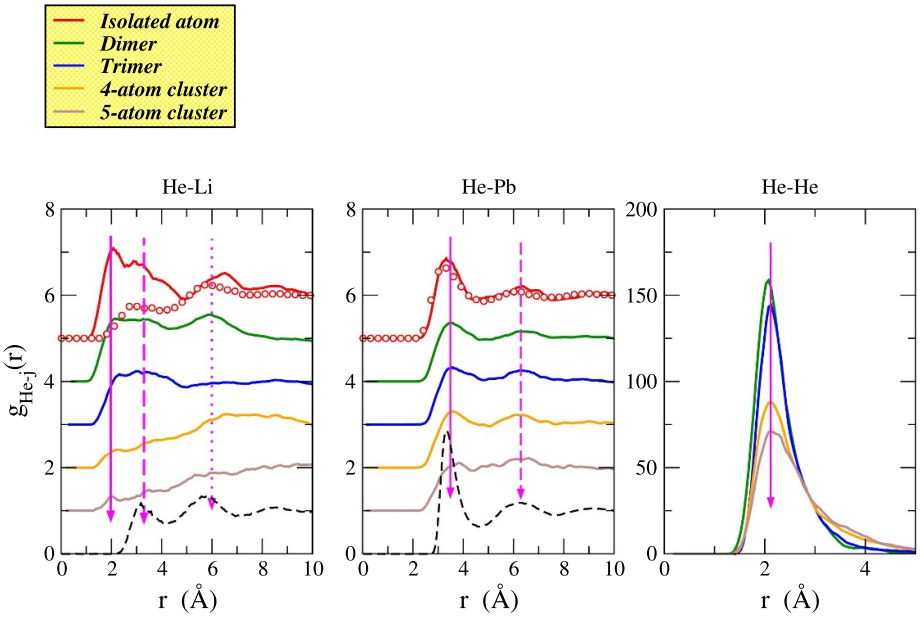


**Figure 10.** Pair correlation functions, $g^{(n)}_{\mathrm{He},j}(r)$, corresponding to He atoms belonging to $n$-atom clusters. The simulation results have been smoothed through short running averages and have been displaced upwards to improve visibility. The Li–Li (left panel) and Pb–Pb (central panel) pair correlation functions are also shown with dashed lines for reference. Circles represent the results obtained by Alvarez-Galera *et al* [20] using effective interatomic potentials.

Within VASP it is not possible to compute a local pressure so as to obtain a pressure profile inside the cluster (or outside, in the liquid LLE region). However we can resort to some parametrized equation of state (EOS) for He. As far as we know none of the EOS available in the literature covers the range of density and temperature observed within the cluster. In any case, taking the density of the cluster at its centre and extrapolating the validity of the EOS of Mills *et al* [35], which was designed to be applicable up to 300 K, to the actual temperature of our system (775 K), this leads to an internal pressure of 18 kbar. Assuming that far from the He cluster the pressure of the LLE is equal to the system pressure, which is close to zero (see table 1), and a radius as obtained from the tanh fit, the Young–Laplace equation, $P_{\mathrm{He}} - P_{\mathrm{LLE}} = 2\gamma_{\mathrm{LLE-He}}/R$, would lead to an interfacial tension, $\gamma_{\mathrm{LLE-He}} = 408 \times 10^{-3}\,\mathrm{N\,m^{-1}}$. If we use instead the radius associated to the equimolar surface, obtained from the relation [36]

$$R_e^3 = \frac{\int \mathrm{d}r r^3 \rho'(r)}{\int \mathrm{d}r \rho'(r)}, \tag{8}$$

where the prime denotes the derivative, which gives $R_e = 4.76$ Å, then the value of the interfacial tension would be $\gamma_{\mathrm{LLE-He}} = 430 \times 10^{-3}\,\mathrm{N\,m^{-1}}$. In view of all the approximations involved, taking into account that the interface of the liquid LLE alloy occurs with He and not with its own vapour, and that the interface is spherical instead of planar, the values obtained for $\gamma_{\mathrm{LLE-He}}$ are in reasonable agreement with the experimental planar surface tension of the LLE alloy at 775 K [11], $\sigma_{\mathrm{LLE}} = 449 \times 10^{-3}\,\mathrm{N\,m^{-1}}$.

We have also computed the pair correlation functions around a He atom, when this atom is part of an $n$-atom He cluster, $g^{(n)}_{\mathrm{He},j}(r)$, using the MD configurations during which any such $n$-cluster is stable. Figure 10 displays these $g^{(n)}_{\mathrm{He},j}(r)$ for $n = 1, \cdots, 5$ and $j$ being Li, Pb or He. Note that some of these functions are rather noisy due to the very small number of He atoms involved and to the limited stability time of the clusters. Nevertheless, some features can still be discerned concerning the preferred He-$j$ distances and their evolution as the cluster grows. We observe that the typical distance from the He atoms to Li or Pb atoms, as characterized by the positions of the maxima of the corresponding pair correlation functions, do not change with cluster size, while the amplitudes tend to diminish as a consequence of the incorporation of He neighbours that displace Li or Pb. Interestingly the shortest typical distance is that of He–Li pairs, followed closely by He–He pairs, and then, for quite longer distance, He–Pb, whose typical distance is in fact close to that of Pb–Pb pairs.

Comparison of the pair correlation function between isolated He atoms and Li or Pb obtained in this study with those obtained by Alvarez-Galera *et al* in their study of solubility of He in the LLE alloy [20] reveals important discrepancies in the case of the He–Li correlation function, while the He–Pb functions are quite similar. Our AIMD computed $g^{(1)}_{\mathrm{He,Li}}(r)$ shows a first peak just below 2 Å, with a shoulder

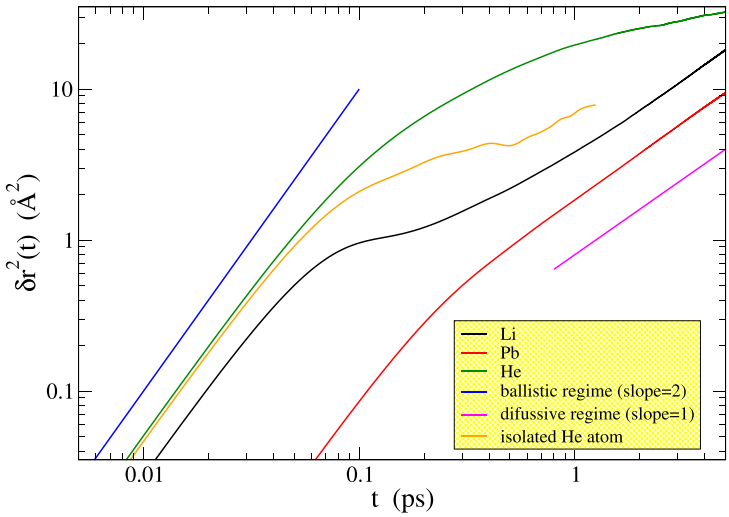


**Figure 11.** Atomic mean squared displacements in the LLE+He system. The orange line corresponds to isolated He atoms. The blue and magenta lines have slopes 2 and 1, to be used as references for ballistic and diffusive regimes respectively.

of relatively high intensity just above 3 Å, and a second peak around 6 Å. The corresponding function obtained with effective pair potentials, displayed only a small peak of height smaller than unity in the region of our main peak, whereas the second peak is similar to the AIMD one [20]. These differences must be attributed to the He–Li interaction model used in the simulations of Alvarez-Galera *et al*, and highlight the potential transferibility problems that can be faced by effective potentials.

### 4.2. Single-particle dynamics

We have computed the mean squared displacements of Li, Pb and He atoms from the configurations generated in the AIMD run. The results are plotted in a log–log scale in figure 11. In this type of graph it is easy to recognize the ballistic behaviour at short times, where $\delta r^2(t)$ varies quadratically with time, leading to a straight line with slope 2, and the diffusive regime at long times, where the mean square displacement is linear in time, which leads in the log–log plot to a straight line with slope 1.

We observe that, contrary to Li and Pb, He atoms do not reach a diffusive behaviour even for quite long times, as the slope of the curve in figure 11 is clearly smaller than 1. This is therefore a sub-diffusive regime, that we ascribe to the limited space available for He atomic motion when the atoms are confined inside the aggregate. If we select for the calculation of $\delta r^2(r)$ only atoms that do not belong to any He cluster, i.e. isolated He atoms, then the corresponding mean squared displacement does become diffusive at long times, although it has much poorer statistics than the Li and Pb counterparts, leading to larger uncertainty in the estimated diffusivity. The diffusion coefficients for Li, Pb and isolated He atoms, as obtained from the slopes of the corresponding $\delta r^2(r)$, are $D_{\mathrm{Li}} = 0.55 \pm 0.05$, $D_{\mathrm{Pb}} = 0.32 \pm 0.03$ and $D_{\mathrm{He}} = 0.90 \pm 0.30$ Å$^2$ ps$^{-1}$, respectively. The two former are in good agreement with the values for the pure LLE alloy [29], namely, 0.52 and 0.33 Å$^2$ ps$^{-1}$ respectively.

## 5. Conclusions

Concerning LLE+T systems, we highlight that the strong interaction of tritium with Li induces some Li atoms to leave the neighbourhood of Pb atoms and join T (and $T_2$ molecules when they exist). This has important effects on the structural and vibrational properties of these species. On the contrary, the structural arrangement of Pb atoms is hardly affected by the presence of tritium in the system.

We find that tritium molecules, $T_2$, can exist dissolved in the bulk LLE alloy for times long enough to be considered as a fourth component of the mixture. Obviously this can only happen if the tritium concentration is large enough so that the probability of finding two tritium atoms close together is not negligible. The fact that Pb is not a metal especially active for hydrogen dissociation and that $T_2$ molecules on average are connected to only one Li atom may explain the unexpected survival of these molecules within the liquid. Note that the existence of $T_2$ molecules within the liquid LLE alloy, despite

being scientifically interesting, is very unlikely to have a technological impact in the real operating conditions of the breeding blanket in fusion reactors, since the expected tritium concentration, around one appm, is much lower than those studied in this work, and this reduces drastically the probability that two T atoms encounter each other and bind together. Nevertheless, in the extremely unlikely case that the molecule formed, its lifetime would be expected to be similar to those observed in this study, since its dissociation mechanisms would be equally unfavourable.

Those Li atoms bound to T display a coordination number around 1, while T atoms are coordinated on average with 3 Li atoms. At high pressure and tritium concentration tritium molecules also bind with roughly one Li atom. However, at lower pressures, when they exist, $T_2$ molecules show a very diffuse coordination structure and it is difficult to define a first coordination shell to analyse the number and type of neighbours of the molecules.

The vibrational spectra of the different species show peaks at different frequencies as expected due to their different masses, but additionally tritium shows another peak at the typical frequency of Li, due to their strong interaction. Moreover, when $T_2$ molecules are present their stretching mode shows up as another high frequency peak in the power spectrum. This stretching frequency decreases upon compression, reflecting the stronger interaction of the molecules with Li atoms as a result of the decrease in their relative distance.

Observing the variation of the properties studied upon lowering T concentration we would expect the following behaviour in the extremely diluted case of the operating blanket. (i) Most of the Li atoms would not be coordinated to T, and therefore, globally the Li–Li pair correlation function would not show the large increase in amplitude observed in this study, nor the Li–Pb correlation function show the related decrease in its height. (ii) The first coordination shell of T atoms would have an extent similar to that obtained in the present study, which was independent of T content, and it would likely contain three Li atoms. And (iii) the characteristic vibration frequencies of Pb, Li and T atoms would keep similar values as obtained here, including the Li–T coupling observed in this study. These expectations can only be confirmed by performing simulations at much higher dilution, which indeed will be performed subsequently using machine learned potentials trained with the present AIMD simulations.

Concerning the LLE+He system, the main conclusion is that He atoms aggregate in clusters (limited due to the number of He atoms simulated) that are dynamically stable for at least some tens of ps. We can provide interesting properties of the 26-atom He aggregate formed in the system, such as its radius or its internal density. Another interesting observation is that, for this He concentration, the He–Li distance is a little shorter than the He–He one, while the He–Pb distance is rather longer. This is an important characteristic property that should be taken into account if model interatomic potentials are to be developed. The properties, both structural and dynamic, of the underlying LLE alloy hardly change upon addition of He. Finally, we observe that He atoms in general show a subdiffusive behaviour, while isolated He atoms display a high diffusivity.

Upon dilution towards the appm level expected in the operating blanket, isolated He atoms are expected to show a longer lifetime, although eventually they would cluster together and possibly form thermodynamically stable bubbles. A simulation at lower He concentration, again using machine learned potentials, will allow a more precise characterization of the diffusivity of atomic He still keeping the high accuracy of first principles calculations, which cannot be guaranteed for effective potentials.

## Acknowledgments

The financial support of the spanish AEI (Ministerio de Ciencia, Innovacion y Universidades) through Grant PID2024-159263NB-I00 is gratefully acknowledged. BGR additionally acknowledges the funding received from the Spanish Ministry of Universities through the Maria Zambrano program partly funded by NextGenerationEU funds.

## Data availability statement

The data that support the findings of this study are openly available at the following URL/DOI: https://uvadoc.uva.es/handle/10324/81120 [43].

## Author contributions

Beatriz G del Rio 0000-0002-1641-8407
Conceptualization (equal), Funding acquisition (equal), Investigation (equal), Methodology (equal), Validation (equal), Writing – review & editing (equal)

Joël Martín Dalmas 0009-0002-0079-3402
Data curation (equal), Investigation (equal), Visualization (equal), Writing – review & editing (equal)

Nonia Vaquero-Sabater 0009-0005-7060-0786
Data curation (equal), Investigation (equal), Visualization (equal), Writing – review & editing (equal)

David J González 0000-0003-1116-3473
Conceptualization (equal), Funding acquisition (equal), Investigation (equal), Methodology (equal), Supervision (equal), Validation (equal), Writing – review & editing (equal)

Luis E González 0000-0001-6264-8329
Conceptualization (equal), Funding acquisition (equal), Investigation (equal), Methodology (equal), Resources (equal), Supervision (equal), Validation (equal), Writing – original draft (equal), Writing – review & editing (equal)

## Appendix. Dissociation of molecular tritium in the liquid LLE alloy.

The $H_2$ molecule is characterized by a doubly occupied bonding $\sigma_g$ molecular orbital and an empty antibondig $\sigma_u^*$ orbital. Its binding energy is relatively high, around 4.5 eV, reflecting its substantial stability. For dissociation to occur through interaction with an external system, several conditions should be satisfied: (i) significant orbital overlap between the molecular orbitals of $H_2$ and the electronic states of the interacting system, (ii) electronic charge transfer into the antibonding $\sigma_u^*$ orbital, and (iii) formation of sufficiently strong bonds between the interacting system and the resulting hydrogen atoms to compensate energetically for the cost of breaking the H-H bond.

The most common scenario for $H_2$ dissociation arises when the molecule approaches the surface of a metal. However, not all metals exhibit dissociative activity. Transition metals with partially filled *d* bands, such as Pd or Pt, are particularly effective in dissociative chemisorption of hydrogen. In contrast, noble metals, with fully occupied *d* bands display significantly lower activity. Unoccupied *d* states play a crucial role in reducing the activation barrier for dissociation [37] and in enabling hybridization that enhances orbital overlap and facilitates occupation of the antibonding $\sigma_u^*$ orbital, thereby weakening the H–H bond [38].

In the LLE alloy *d* bands are either absent (Li) or inert (Pb). Consequently, any dissociation process must proceed through alternative mechanisms. In the case of Li, the main route involves charge transfer. Owing to its strong electropositive character, Li readily donates electrons to $H_2$, which then populate the antibonding $\sigma_u^*$ orbital. The associated energetic cost is compensated by the formation of relatively strong, predominantly ionic Li–H bonds, with a binding energy of approximately 2.5 eV. Note, however, that at least two Li atoms must participate in the process, since a single Li atom can donate at most one electron, which is insufficient to effectively destabilize the H–H bond. Explicit calculations showed that a $Li_4$ cluster readily dissociates $H_2$ [39], but for a system formed by one Li atom and two H atoms the ground state of $Li+H_2$ is more stable than that of LiH+H [40]. Indeed, decoration of carbon-based sheets with spatially separated Li atoms bound to the substrate has been proposed as a promising strategy for efficient hydrogen storage via physisorption of $H_2$ molecules, i.e. without molecular dissociation (see, for instance, [41]).

The situation for Pb differs substantially from that of Li. Pb is significantly less electropositive, the Pb–H binding energy is lower (approximately 1.8 eV), and the orbital overlap between Pb *p* states and the molecular orbitals of $H_2$ is limited. As a consequence, Pb surfaces are expected to exhibit low efficiency for $H_2$ dissociation. This expectation has been confirmed in studies of the Pb(111) surface [42], where adsorbed $H_2$ molecules were found to be more stable than two separately adsorbed hydrogen atoms.

We consider now a $T_2$ molecule formed inside the liquid LLE alloy. Its interaction with Pb is intrinsically weak, as commented above, which is also attested by the form of the $T_2$–Pb pair correlation functions (see figure 3). Furthermore, the average number of Li atoms coordinated to a $T_2$ molecule is approximately one (see table 2). These two factors may account for the relatively long lifetime of $T_2$ molecules in the liquid phase. Dissociation is expected to occur only when atomic motion within the

liquid brings at least two Li atoms into close proximity to the molecule, enabling sufficient charge transfer to break the bond.

## References


[1] Tokimatsu K, Hondo H, Ogawa Y, Okano K, Yamaji K and Katsurai M 2000 *Fusion Eng. Des.* **48** 483
[2] Chadwick M B *et al* 2024 *Fusion Sci. Technol.* **80** S9
[3] Lucas L L and Unterweger M P 2000 *J. Res. Natl Inst. Stand. Technol.* **105** 541
[4] Hernández F A and Pereslavtsev P 2018 *Fusion Eng. Des.* **137** 243
[5] Hesch K, Boccaccini L V and Stieglitz R 2018 *Kerntechnik* **83** 241
Boccaccini L V *et al* 2022 *Fusion Eng. Des.* **179** 113116
[6] Federici G, Biel W, Gilbert M R, Kemp R, Taylor N and Wenninger R 2017 *Nucl. Fusion* **57** 092002
[7] Malang M and Mattas R 1995 *Fusion Eng. Des.* **27** 399
[8] Delaporte-Mathurin R, Dark J, Ferrero G, Hodille E A, Kulagin V and Meschini S 2024 *Int. J. Hydrog. Energy* **63** 786
Dark J 2024 Multiphysics tritium transport simulations of the WCLL breeding blanket for DEMO *PhD Thesis* Université Sorbonne Paris Nord
[9] Conrad R 1991 *Fusion Eng. Des.* **14** 289
Conrad R, Rainer L, Coen V and Flament T 1991 *J. Nucl. Mater.* **179–181** 875
[10] Mas de les Valls E, Sedano L A, Batet L, Ricapito I, Aiello A, Gastaldi O and Gabriel F 2008 *J. Nucl. Mater.* **376** 353
[11] Martelli D, Venturini A and Utili M 2019 *Fus. Eng. Des.* **138** 183
[12] Peñalva I, Urrestizala M, Azkurreta J, Alegría N, Malo M, Garcinuño B, Patiño J and Rapisarda D 2024 *Fusion Eng. Des.* **199** 114136
[13] Shibuya Y, Aida M, Fujii Y and Okamoto M 1987 *J. Nucl. Mater.* **150** 286
[14] Reiter F 1991 *Fusion Eng. Des.* **14** 207
[15] Terai T, Nagai S, Yoneoka T and Takahashi Y 1992 *J. Nucl. Mater.* **187** 247
[16] Kobayashi M, Hamada A, Matsuoka K, Suzuki M, Osuo J, Edao Y, Fukada S, Yamanishi T, Oya Y and Okuno K 2017 *Fusion Sci. Technol.* **62** 56
[17] Sedano L, Esteban G A, Cavaro M, Iraola E, Abdulrahman A, Batet L and Guasch M 2022 *Nucl. Mater. Energy* **31** 101185
[18] Masuyama D, Oda T, Fukada S and Tanaka S 2009 *Chem. Phys. Lett.* **483** 214
[19] Fraile A and Polcar T 2020 *Nucl. Fusion* **60** 046018
[20] Álvarez-Galera E, Laria D, Mazzanti F, Batet L and Martí J 2025 *J. Mol. Liq.* **432** 127719
[21] Al-Awad A S, Batet L, Rives R and Sedano L 2024 *J. Chem. Phys.* **161** 024503
[22] Wang G, Wang C, Zhang X, Li Z, Zhou J and Sun Z 2024 *iScience* **27** 109673
[23] Arena P *et al* 2021 *Appl. Sci.* **11** 11592
[24] Hohenberg P and Kohn W 1964 *Phys. Rev.* **136** B864
[25] Kohn W and Sham L J 1965 *Phys. Rev.* **140** A1133
[26] Kresse G and Hafner J 1993 *Phys. Rev. B* **47** 558
Kresse G and Hafner J 1994 *Phys. Rev. B* **49** 14251
Kresse G and Furthmuller J 1996 *Phys. Rev. B* **54** 11169
Kresse G and Furthmuller J 1996 *Comput. Mater. Sci.* **6** 15
[27] Perdew J P, Burke K and Ernzerhof M 1996 *Phys. Rev. Lett.* **77** 3865
[28] Blochl P E 1994 *Phys. Rev. B* **50** 17953
Kresse G and Joubert D 1999 *Phys. Rev. B* **59** 1758
[29] Alemany M M G, Souto-Casares J, González L E and González D J 2021 *J. Mol. Liq.* **344** 117775
[30] del Rio B G and González L E 2023 *J. Chem. Phys.* **159** 234502
[31] Li D, Zhang Y G, He H Y, Liu C S and Pan B C 2015 *J. Nucl. Mater.* **467** 181
[32] Chen M, Abrams T, Jaworski M A and Carte E A 2016 *Nucl. Fusion* **56** 016020
[33] del Rio B G, Gautam G S and Carter E A 2020 *Nucl. Fusion* **60** 016025
[34] Lai K-F, Hermann V, Trivikram T M, Diouf M, Schlösser M, Ubachs W and Salumbides E J 2020 *Phys. Chem. Chem. Phys.* **22** 8973
[35] Mills R L, Liebenberg D H and Bronson J C 1980 *Phys. Rev. B* **21** 5137
[36] Lovett R and Baus M 1997 *J. Chem. Phys.* **106** 635
[37] Harris J and Andersson S 1985 *Phys. Rev. Lett.* **55** 1583
[38] Siegbahn P, Blomberg M, Panas I and Wahlgren U 1989 *Theor. Chim. Acta* **75** 143
[39] Przybylski K, Koutecký J, Bonačić-Koutecký V, von Ragué-Schleyer P and Guest M F 1991 *J. Chem. Phys.* **94** 5533
[40] Wernli M, Caruso D, Bodo E and Gianturco F A 2009 *J. Phys. Chem. A* **113** 1121
[41] Cabria I, Lebon A, Torres M B, Gallego L J and Vega A 2024 *Int. J. Hydrog. Energy* **57** 26
[42] Saalfrank P, Juaristi J I, Aldućin M, Blanco-Rey M and Diez Muiño R 2014 *J. Chem. Phys.* **14** 234702
[43] del Rio B G, Martin Dalmas J, Vaquero Sabater N, Gonzalez D and Gonzalez L E Research data for "Structure and motion of tritium and helium in the breeding-blanket-relevant liquid lithium-lead eutectic alloy: ab-initio molecular dynamics simulations *UVaDOC. Repositorio documental de la Universidad de Valladolid* (available at: https://uvadoc.uva.es/handle/10324/81120)